NEUROSCIENCE

Beyond nature, nurture, and chance: Individual agency shapes divergent learning biographies and brain connectome

Warsha Barde[1,2]†, Jonas Renner[1,2]†, Brett Emery[1], Shahrukh Khanzada[1], Xin Hu[1], Alexander Garthe[1,2], Annette E. Rünker[1,2], Hayder Amin[1], Gerd Kempermann[1,2]*

Individual choices shape life course trajectories of brain structure and function beyond genes and environment. We hypothesized that individual task engagement in response to a learning program results in individualized learning biographies and connectomics. Genetically identical female mice living in one large shared enclosure freely engaged in self-paced, automatically administered and monitored learning tasks. We discovered growing and increasingly stable interindividual differences in learning trajectories. Adult hippocampal neurogenesis and connectivity as assessed by a high-density multielectrode array positively correlated with the variation in exploration and learning efficiency. During some tasks, divergence transiently collapsed, highlighting the sustained significance of context for individualization. Thus, equal environments and equal genes do not result in equal learning biographies because life confronts individuals with choices that lead to divergent paths.

INTRODUCTION

Interindividual differences in behavior and underlying brain physiology are pervasive throughout the animal kingdom, reflecting the fundamental interplay of genetic, environmental, and developmental factors (*1*, *2*). Despite the ubiquity of these differences, the precise mechanisms underlying the emergence of individuality remain elusive and complex. While the debate on nature versus nurture has long dominated discussions on individual variation, newer research indicates that individuality extends beyond such a narrow dualistic framework. Environmental enrichment (ENR) has been a paradigm of choice to study gene × environment interactions by controlling the genetics using inbred mice. We have shown that genetically identical mice living together in the same environment still develop divergent behavioral trajectories (*3*). Given the shared genetic background and macroenvironment, only the nonshared environmental factor, i.e., the component of differential behavior, remained as potential catalysts for the emergence of individuality. Theories on stochastic experiential variation and noisy developmental processes further emphasize the role of positive feedback loops in amplifying small initial differences (*4*–*6*).

Extending beyond the trichotomy of nature (genes), nurture (environment), and chance, we propose individual agency as a major factor in shaping developmental trajectories. We here present an innovative form of learning-centered ENR that isolates the effects of individual choice, learning, and environmental feedback on the emergence of individual learning biographies and associated neural plasticity.

RESULTS

The IntelliCage acts as an enriched environment

Thirty-two 5-week-old female C57BL/6JRj mice were randomly assigned to either the enriched training environment or standard housing (STD) for 11 weeks (Fig. 1B). The IntelliCage (IC) is a computer-based, fully automated home cage system to longitudinally monitor the exploratory, learning, and social behavior of mice (Fig. 1A) (*7*). In four operant conditioning corners, which are equipped with two nosepoke holes, sweetened water as a reward, and doors that allow or deny access to the reward, mice can freely and at their own pace learn and solve tasks to receive a reward. Access to the reward is based on a predefined combination of visits to specific corners, nosepoke patterns, and animal identity being automatically recorded through radio-frequency identification (RFID) antennas, nosepoke sensors, and lickometers. Of the more than 150 IC publications so far, none has explored long-term and sequential task exposure (*7*). In contrast, we exposed the mice to a nonstop sequence of learning tasks over 2 months. While a gradual increase in body weight was observed in both STD and IC animals (Fig. 1C), IC mice were consistently lighter as one observes in other forms of enrichment (*8*). Like classical ENR, IC also caused an increase in the mean and variance of adult hippocampal neurogenesis (Fig. 1D) (*9*–*11*). These results validate the IC as an effective tool to induce enrichment effects in mice.

Emergence of individuality in behavior

During an adaptation phase (10 days), the mice were familiarized with the enclosure, the rewards in the corners, the requirement for a nosepoke to obtain the reward, and a time restriction for accessing the reward (fig. S1A). The learning phase itself consisted of a total of 10 variations of five learning tasks: place learning with three correct corners (PL3CC); place learning with one correct corner (PL1CC); patrolling where the position of the correct corner shifted either in a clockwise or anticlockwise direction; reverse patrolling where the direction in which the correct corner rotated was reversed; and serial reversal task where initially two diagonally opposite corners were rewarded, and the mice had to shuttle between these corners to access the reward. The assignment of diagonally opposite correct and incorrect corners was reversed every 4 days (fig. S1B).

Roaming entropy (RE) is a metric for uniform territorial coverage and spatial exploration exhibited by individual mice (*10*), also translatable to human conditions (*12*). We used the number of corner visits

[1]German Center for Neurodegenerative Diseases (DZNE) Dresden, Dresden, Germany. [2]CRTD–Center for Regenerative Therapies TU Dresden, Dresden, Germany.
*Corresponding author. Email: gerd.kempermann@dzne.de; gerd.kempermann@tu-dresden.de
†These authors contributed equally to this work.

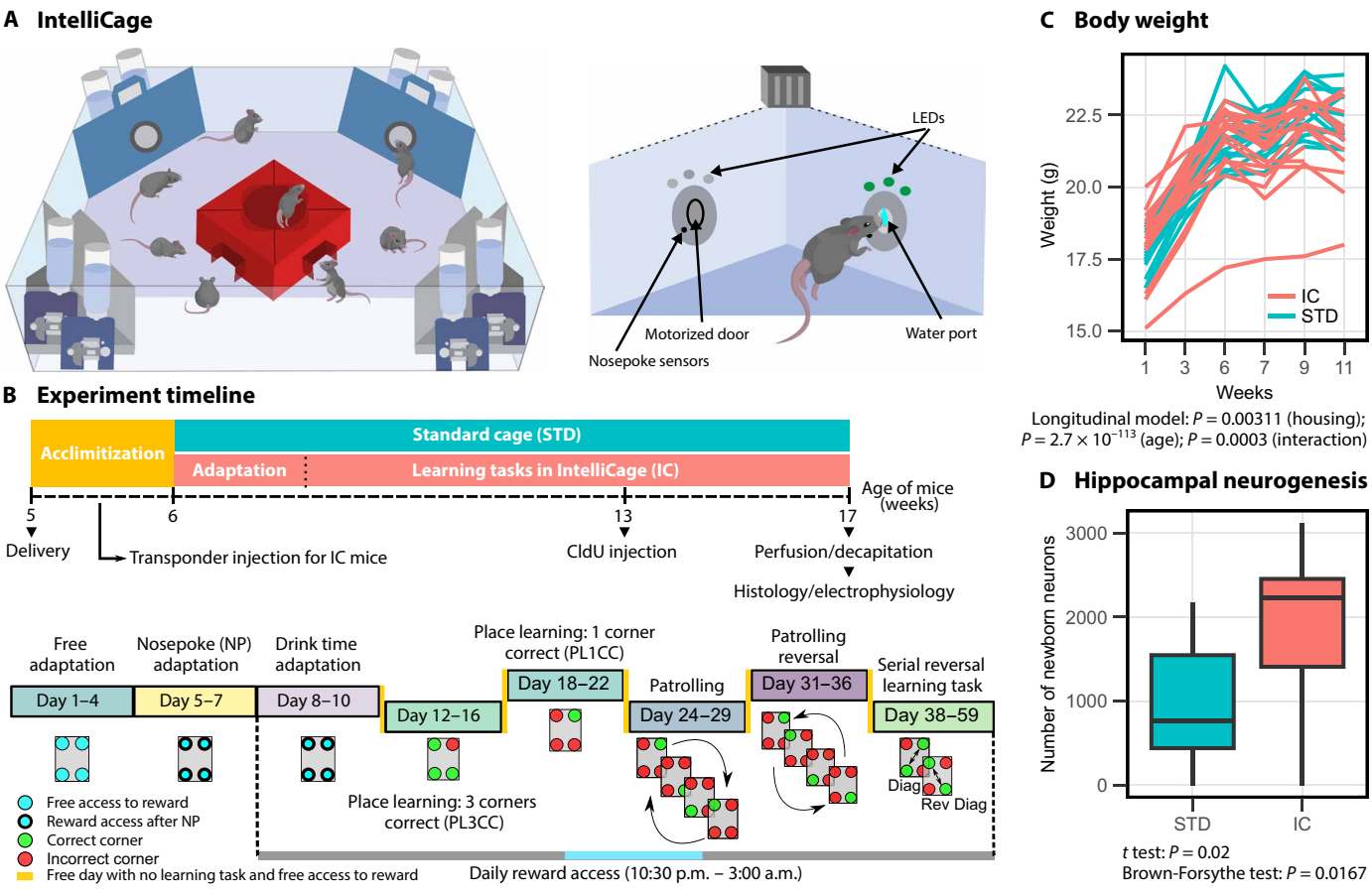

Fig. 1. IC as an enriched environment. (**A**) Schematic representation of IC that can house up to 16 mice and is equipped with four operant conditioning corners with RFID antennas (left). Each corner contains two nosepoke ports with motorized doors, light-emitting diodes (LEDs) above nose ports, and access to sweetened water as a liquid reward behind the door (right). (**B**) Thirty-two female C57BL/6JRj mice, aged 5 weeks, were randomly assigned to IC and STD for 11 weeks. For quantification of adult hippocampal neurogenesis, all mice were injected with the thymidine analog 5-chlorodeoxyuridine (CldU) 4 weeks before the end of the experiment. After the experiment, IC animals were stratified according to their learning performance. The top two learners, the bottom two learners, and two STD mice were used for ex vivo hippocampal electrophysiology. The remaining IC and STD mice were perfused followed by immunohistochemistry to quantify adult hippocampal neurogenesis. (**C**) IC mice had lower body weights compared to STD mice. (**D**) IC mice showed higher mean and variance in the number of new hippocampal neurons compared to STD mice (STD, $n = 14$; IC, $n = 12$). Box and whisker plots: center line, median; upper and lower hinges, first and third quartiles; whiskers, highest and lowest values within 1.5 times the interquartile range (IQR) outside hinges.

and time spent in the corners to calculate RE during the adaptation phase. Decreasing mean RE suggested habituation to the environment (Fig. 2A, middle). Raw as well as cumulative RE trajectories diverged over time (Fig. 2B, right). Thus, during the initial 10 days in the IC, individual behavioral trajectories emerged as described previously for the much larger and elaborate individuality paradigm (*11*, *13*, *14*).

The successive learning tasks progressed in difficulty. Initially, the mice were required to learn the location of rewarded corners. In subsequent tasks, they had to unlearn the previous corner assignments and learn the new locations of rewarded corners. Learning success of individual mice was calculated as the percentage of correct visits, normalized to the chance level (= 0) of the respective task. The resulting learning curves, over the entire learning phase, diverged and increased in variance, demonstrating individualization of the trajectories (Fig. 2B). Within individual tasks, the average performance mostly increased except for "reverse diagonal 1" and "diagonal 3" (Fig. 2C). However, the group-average learning curve does not adequately represent the behavior of individual animals. Individual learning trajectories fanned out even within individual tasks, but there also was a fanning-in of curves in certain tasks (Fig. 2C). Individual mice differed in their baseline performance levels (intercept), learning rates (slope), as well as endpoint performance, and the variance for all three parameters increased (Fig. 2, D to F).

It has been shown that the formation of individual behavioral trajectories in ENR at least in part depends on adult neurogenesis (*14*) and that adult-born neurons facilitate flexible relearning (*15*–*17*). On the basis of this, we calculated the percentage of times mice visited the previously correct corner during a new task (flexibility curves; fig. S2A). On average, this measure decreased over the course of the tasks, except for "reverse patrolling" and reverse diagonal 1. The flexibility curves of individual mice also showed a fanning-out or fanning-in pattern depending on the task. Intercepts, slopes, and endpoints of these curves showed a nonsignificant trend of increase in variance (fig. S1, B to D).

While divergent learning trajectories indicate the amplification of stochastic or other baseline differences through different rates of adaptation to the tasks, the convergence of curves suggests that animals became more similar to each other in their learning outcome,

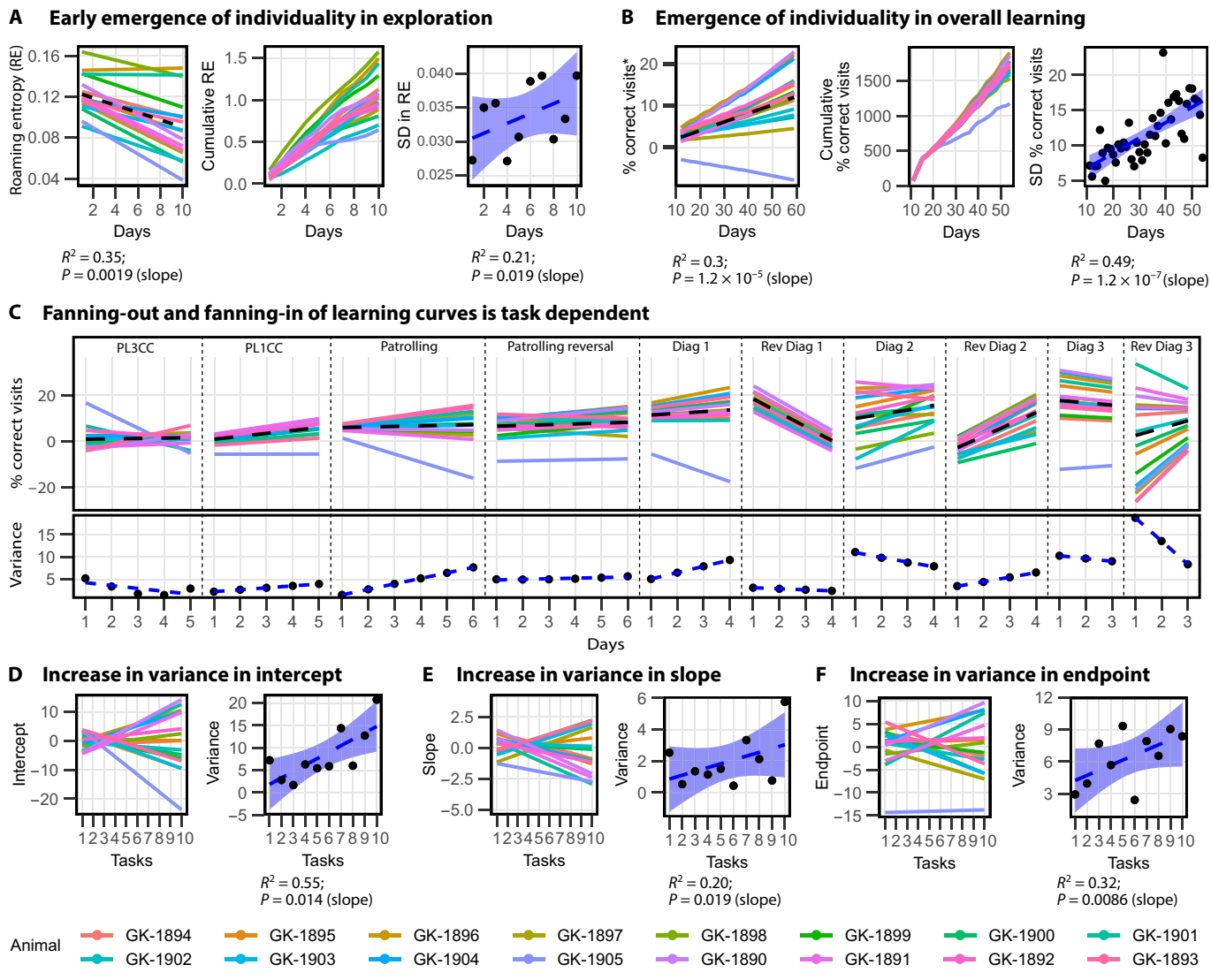

Fig. 2. Emergence of individuality in behavior. (**A**) Individual mouse trajectories for exploratory behavior were assessed by calculating RE by using time spent in corners. The black dashed line indicates the decrease in mean RE, implying habituation to the environment (left). Raw and cumulative RE trajectories (middle) diverged in the adaptation phase indicated also by the significant increase in the SD of REs (right). (**B**) Individual learning curves were derived after centering the percent correct visit values on the chance level of each learning task. The black dashed line indicates a significant increase in learning success at the group level (left). Raw and cumulative learning trajectories (middle) demonstrated divergence over time (left), evident also by a significant increase in SD (right). (**C**) Learning curves centered at chance level, displayed both divergence and convergence depending on the task (top), which corresponded with fluctuations in the variance over the task timescale (bottom). The dashed lines in the top and bottom indicate the mean and variance, respectively, of percent correct visits obtained from linear regression. Refer to table S2 for statistical details. (**D** to **F**) Variance in baseline performance (intercept), rate of learning (slope), and final performance (endpoint) increased as the tasks progressed. Before calculating variance, values of intercept, slope, and endpoint are centered with respect to fixed-effect coefficients specific to each task. The trajectory of each mouse is represented by a colored line, as shown in the bottom, and is derived from a linear mixed-effect model. R^2 and P values are obtained from linear regression. The envelope indicates SE. Legend of learning tasks: Task 1, PL3CC; task 2, PL1CC; task 3, patrolling; task 4, patrolling reversal; tasks 5, 7, and 9, diagonal (Diag); tasks 6, 8, and 10, reverse diagonal (Rev Diag).

despite differences in intercept and slope. In line with the postulate that choice architectures influence behavior (*18*), learning-induced individualization was not uniform but was shaped by the task's structure, dictating the degree of freedom of choices available to the animals.

Stability in the face of change

To assess the stability or predictability of an individual's behavioral pattern over time and across contexts, we quantified how individuals maintained their relative placement or rank order within the group. During the adaptation phase, animals maintained high rank-order correlations in their mean RE suggesting consistent patterns of exploration and habituation (Fig. 3A, left). In the learning phase, for the mean percentage of correct visits, animals exhibited a high level of rank-order consistency between tasks indicating that animals consistently performed relative to one another (Fig. 3A, right). While the "reverse diagonal" tasks exhibited a low correlation with other tasks, they correlated highly with each other, indicating that they shared unique characteristics that led to consistent performance patterns among the animals. In comparison, overall rank-order consistency was low for behavioral flexibility (fig. S2E).

Repeatability, which quantifies the constancy of a feature over time and helps identify stable interindividual differences that surpass intraindividual fluctuations (*19*), gradually increased for exploratory activity, learning, and flexibility (Fig. 3B and fig. S2F). Correspondingly, we observed an increase in interindividual variance in these behaviors (Fig. 3C and fig. S2G), while the intraindividual variance either decreased or remained constant (Fig. 3D and fig. S2H). This suggests that animals become increasingly consistent in their individual behavior that distinguishes them from others while retaining their intraindividual variability.

Individuality in behavior correlates with individuality in brain plasticity

After the experiment, animals were stratified according to their learning performance, and the top two learners, the bottom two learners, and two standard mice were used for electrophysiological analyses. For the remaining mice, adult hippocampal neurogenesis was quantified immunohistochemically. We found a trend for a positive correlation between mean RE and the number of newborn neurons in the dentate gyrus (DG), suggesting that animals who explore more tend to grow more neurons in their hippocampus (Fig. 4, A and C), in line with earlier work (*11*). The weak correlation can be explained by the short recording time for RE (first 10 days), while the neurogenesis counts cover the last 4 weeks. Adult hippocampal neurogenesis positively correlated with both learning and flexibility (Fig. 4, B and C, and fig. S2I).

Building on our previous work on the effects of ENR on hippocampal circuitry (*20*), ex vivo electrophysiology using a high-density (HD) microelectrode array (MEA) [complementary metal-oxide semiconductor (CMOS) based] detected substantial subregion-specific differences in local field potential (LFP) amplitude between the individuals in the different experimental conditions (Fig. 4, D and E). To examine synaptic plasticity, evoked field excitatory postsynaptic potential (fEPSP) amplitude responses were recorded through electrical stimulation of the stratum radiatum of the cornu ammonis 1 (CA1) subregion to activate the Schaffer collateral (SC) pathway. Comparing the tuning curves assessed the range of synaptic plasticity. The increased fEPSP evoked amplitude response in the top learning mice, compared to standard or bottom learning mice, suggested that the synaptic connections exhibited greater responsiveness or sensitivity to changes in the stimulation parameters (Fig. 4J and fig. S4A). This indicates that the synapses are more capable of undergoing potentiation in response to certain stimulation patterns and also have a higher capacity for synaptic strengthening and plasticity of neuronal circuits. This heightened capacity for plasticity might be associated with improved learning and memory formation (*21*). Furthermore, IC top learning mice showed

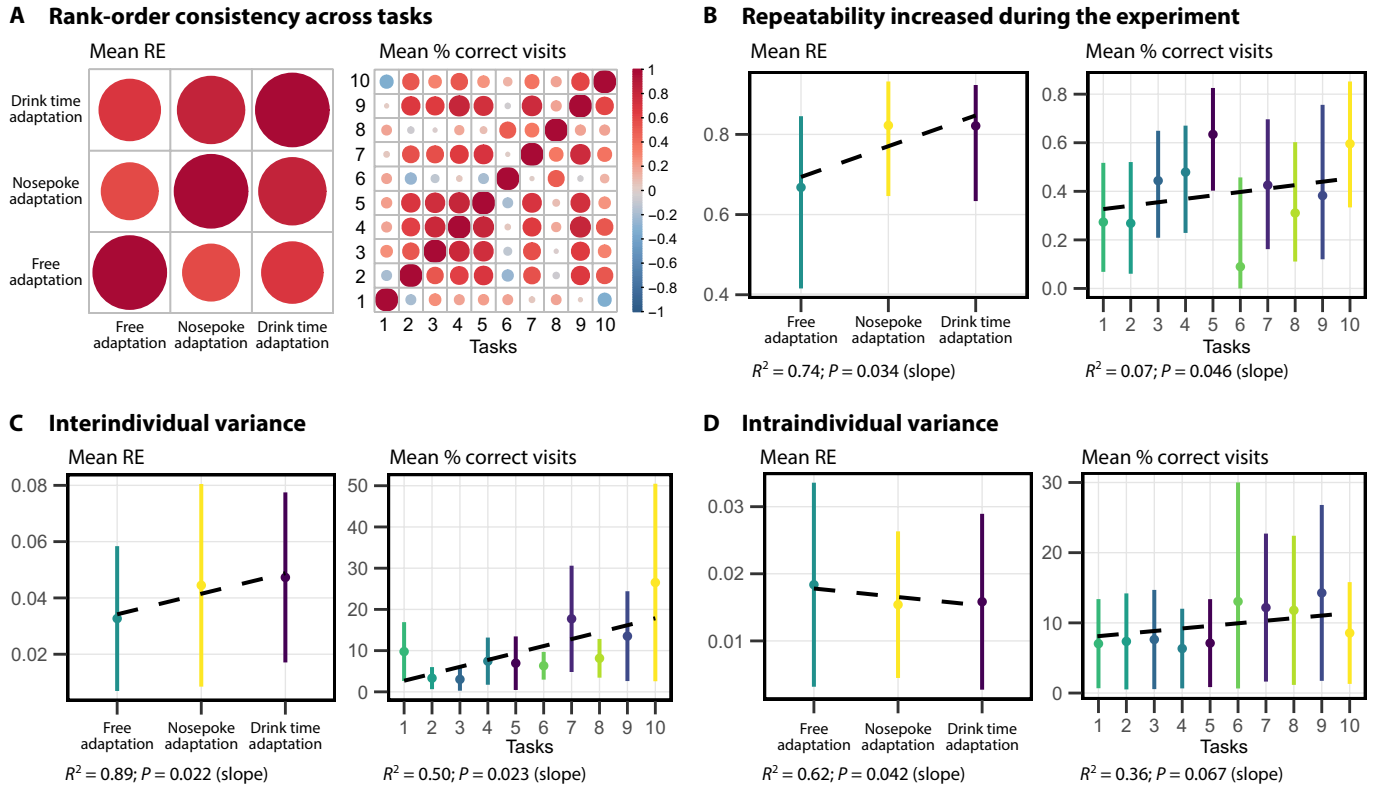

Fig. 3. Stability in individual differences. (**A**) Mean RE showed high rank-order correlations between different phases of the adaptation period (left). In the learning behavior, rank-order consistency was generally high between tasks except for reverse diagonal tasks (6, 8, and 10) (right). Color code and circle size highlight the coefficient of Spearman correlation. (**B**) Repeatability increased for exploratory activity (left) and learning (right) over the adaptation phase and learning phase, respectively. (**C**) Interindividual variance for exploratory activity (left) and learning (right) increased. (**D**) Intraindividual differences in exploratory activity decreased (left), while for learning, they remained stable (right). Repeatability and variance estimates were obtained from linear mixed-effect models and shown with 95% confidence intervals (CIs). Refer to tables S1 and S3 for details. The black dashed lines, R^2, and P values are obtained from linear regression. Legend of learning tasks: Task 1, PL3CC; task 2, PL1CC; task 3, patrolling; task 4, patrolling reversal; tasks 5, 7, and 9, diagonal; tasks 6, 8, and 10, reverse diagonal.

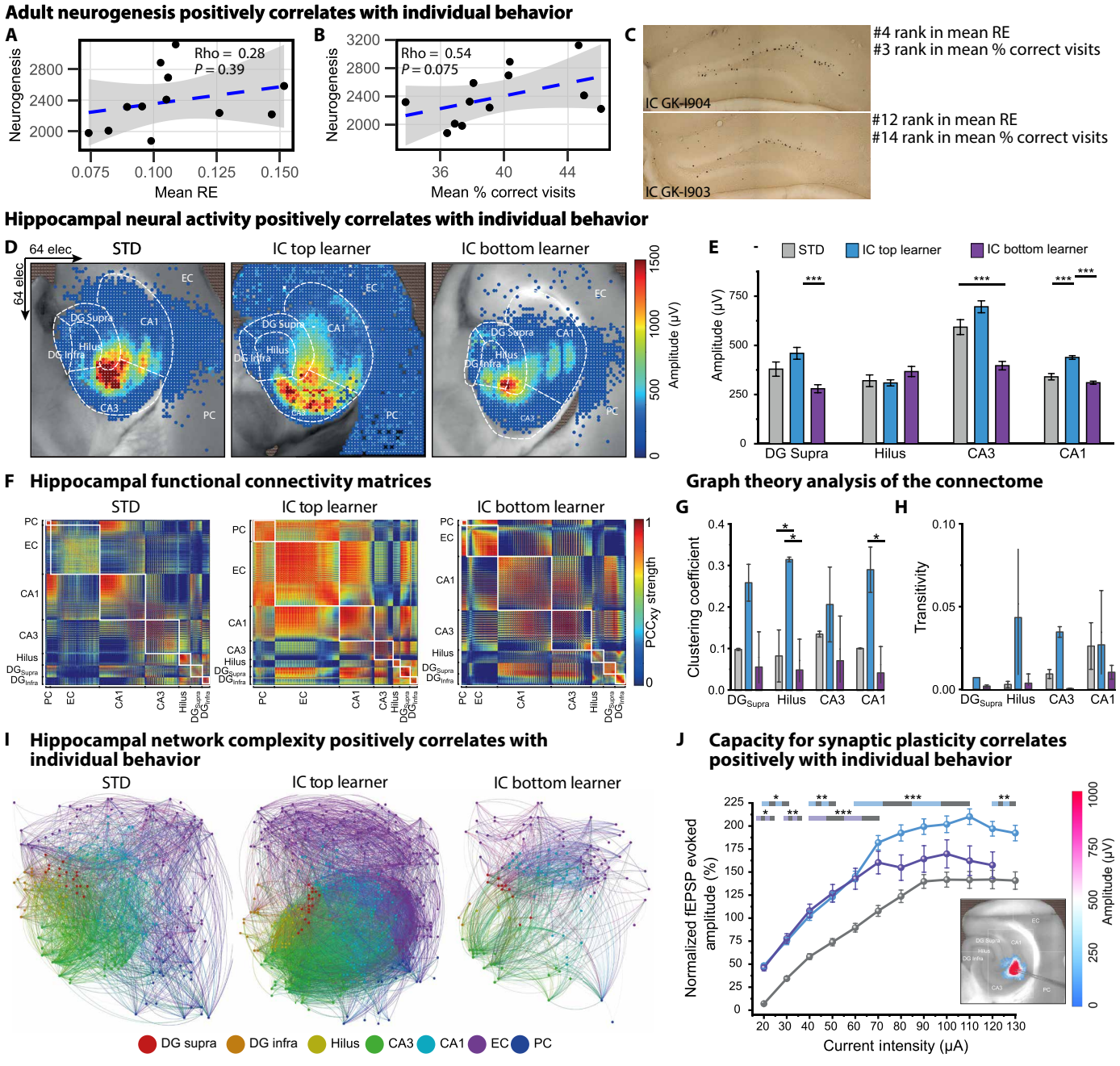

Fig. 4. Individuality in brain plasticity. (**A** and **B**) Adult hippocampal neurogenesis correlates with mean levels of exploration and learning. (**C**) Immunohistochemical detection of CldU-positive cells. (**D**) Topographical pseudo-color mapping of mean LFP amplitude spatial maps, computed over 5-min recordings, superimposed on the light-microscopic image. (**E**) Statistical quantification of the pharmacologically induced spontaneous spatiotemporal firing activity illustrates significantly higher regional LFP amplitude in top learners. (**F**) Functional connectivity matrices representing cross-correlation of pairs of firing neurons. The top learner displays higher correlation in all networks. White squares located along the diagonal illustrate modular graphs with highly connected nodes. (**G** and **H**) Graph clustering coefficient and transitivity indicate higher network segregation in the top learner networks. (**I**) Connectome mapping and network visualization of the hippocampal-cortical (HC) networks. To illustrate exemplary functional connectivity from the dynamic detected LFP events in STD (node = 2701 and links = 123,623), IC top learner (node = 2988 and links = 157,176), and IC bottom learner (node = 2391 and links = 80,178) similar dynamic timeline (100 s) and degree range (>10 functional links per node) parameter constraints were placed on the functional links for plotting each condition. Nodes are scaled according to degree strength with nodal color indicating layer and link color identifying the intra- and interlayer connections. (**J**) Statistical quantification of the stimulation-evoked responses obtained as tuning curve of fEPSP slope amplitude as function of stimulus intensities. Tuning curves were averaged across all evoked electrodes to determine response amplitude with 10-μA pulse intensity difference from 20 to 130 μA and 140-μs pulse width and 30-s time interval between pulses. Inset shows topographical pseudo-color mapping of CA3/CA1 regionally evoked peak-to-peak amplitude spatial maps, obtained from an 80-μA electrical stimulation, superimposed on the HC microscope light image [***$P < 0.001$, **$P < 0.01$, and *$P < 0.05$, analysis of variance (ANOVA)]. DG Supra, DG suprapyramidal; DG Infra, DG infrapyramidal.

significantly higher strength of local and global spatial interactions, as shown in the cross-correlograms (Fig. 4F).

In addition, the hippocampal networks of the IC top learners exhibited higher uni- and bidirectional interaction link counts than those of STD mice, while the networks from IC bottom learners showed a decreased interaction link count compared to both STD mice and IC top learners (Fig. 4I and fig. S4B). The top learners' functional networks showed a higher complexity (Fig. 4I), had more edges, and a higher degree centrality (fig. S4, D and E). On the basis of the clustering coefficient and transitivity, the top learner's networks were more segregated (Fig. 4, G and H), suggesting that the connectome is more modular, which is consistent with the idea that less segregated networks, as associated with cognitive aging, are more vulnerable and less functional (*22*, *23*). Last, the average shortest path length was shorter for the networks of both the IC top and bottom learners compared to those of the STD mice, indicating a greater network integration (fig. S4F) (*24*).

DISCUSSION

The convergence and divergence of behavioral trajectories were not observed in our previous experiments with conventional and more stable ENRs, which lack the dynamic changes in reward contingencies and learning demands that the IC-based enrichment offers. A new level of complexity arises from potential feedback loops between exploratory, social, and learning behaviors, intertwined with their reliance on task-specific constraints. Theoretically, positive and negative state-behavior feedback loops have been shown to lead to divergence and convergence of behavioral trajectories (*25*). An intriguing observation is that after converging phases, during which individuality is reduced to a level of lower performance, upon a new task, the mice switch back to a wider range of starting points into the next task. The shared environment, i.e., the learning situation, thus continues to matter, but the same stimulus can elicit different responses based on past experience.

At the center of our study lies a within-group comparison toward an identical intervention. This is conceptually challenging: The intervention is shared, but the response is increasingly individualized. Nevertheless, the intervention (the task) still originates from the outside and is imposed on the individual. The cross-sectional comparison that we included into our study simply shows that, irrespective of the within-group variability and the role of the nonshared environment, there is a group-level effect that compares to what has been described in many studies on enriched environments in the past (*26*).

The "variation in variability" suggests that the emergence of individual differences is not fixed or predetermined but is nonlinear and dynamic and contingent upon environmental demands and contextual factors. For instance, when faced with challenging tasks, some individuals may exhibit adaptive responses, such as increased perseverance or exploration, while others may show decreased motivation or avoidance. These shifts in behavior can lead to divergent or convergent trajectories in learning biographies, depending on the nature of the environmental feedback.

For the current as well as our previous studies, a linear model has been the best fit, but first unpublished data suggest that, over extended periods of time, an exponential model might become the better fit. While this remains to be confirmed, it is important to note that, on the basis of the present data, we cannot claim a general linear relationship.

The idea of a dynamic interplay between individual choice and actions on one hand, and environmental opportunities and demands on the other, challenges theories that attribute individual differences solely to stochastic or noisy developmental processes, highlighting the active role of individuals in shaping their own life trajectories.

It is not possible to further disentangle the mechanistic nature of this effect: To which extent the reward for learning versus learning per se is the driving stimulus cannot be determined. However, reward is given for a particular learning performance, so that in any case a link to learning can be made. It is conceivable that purely triggering the dopaminergic system, as in the self-administrating models in addiction research, might create some within-group variability as well, but such "individuality" would be independent of learning. We here show that learning, possibly in part through the reward system, induces individualized trajectories.

To further determine whether the variance observed in our data was driven by learning reinforcement or merely by the amplification of initial stochastic differences through developmental noise, we compared a "reinforcement model" with two "null models" using a bootstrap analysis with baseline differences and reinforcement factors derived from experimental data. The null models included a random walk model, where trial success varied randomly around initial differences, and an additive noise model, where success was the sum of previous success plus noise, simulating the emergence of interindividual differences through stochastic development. Across 1000 bootstrap simulations, the mean difference in slope for change in variance between the reinforcement and random walk models was 0.1405 [95% confidence interval (CI): 0.06775, 0.20904; $P < 0.001$], and between the reinforcement and additive noise models was 0.10774 (95% CI: 0.03081, 0.18994; $P = 0.003$) (table S6). This indicates that trajectory divergence in the reinforcement model was significantly greater than in the null models (fig. S6, A to C). The reinforcement mechanism introduces variability in the slopes of the individual learning curves, amplifying the initial differences and leading to divergent trajectories. In contrast, the null models lack this reinforcement; without which, the success rate remains largely driven by random fluctuations. As a result, reinforced mice showed significant improvements in average success rates (fig. S6D and table S6) and greater increases in variance compared to the null model mice (fig. S6E and table S6).

We applied a similar approach to explore variance emergence in exploratory behavior using negative reinforcement. In our data, we observed a decrease in mean RE as a result of habituation, yet the trajectories diverged significantly over time. As mice become familiar with the environment, the reduced novelty can function as a form of negative reinforcement. As expected, we observed a divergence in trajectories for negatively reinforced mice (fig. S6, F to H) compared to mice in the null models. Reinforced mice exhibited a significant decrease in mean RE (fig. S6I and table S7), and their increase in variance was significantly higher than that of the null model mice (fig. S6J and table S7). This further supports the idea that reinforcement mechanisms, whether positive or negative, amplify initial differences and drive greater variability in behavioral outcomes compared to stochasticity. The precise role of the brain's reward system (and hence dopaminergic signaling) in this context remains to be studied.

Our results demonstrate that even with uniform genetic background and exposure to identical tasks, individual trajectories in

learning-associated behaviors, such as learning ability, exploration strategies, and flexibility, emerge in the context of a rich choice architecture and are associated with differences in brain plasticity and the hippocampal connectome. The supplement contains the results from a smaller pilot study with the same design that independently confirms the observations reported here (fig. S5). Our results confirm that the development of individuality depends on sources beyond genes and the external environment (*27*). In a previous study, we have shown that exposure to ENR that promotes individualization is also associated with lasting epigenetic changes at gene loci related to adult neurogenesis and brain plasticity (*11*). The positive correlations between learning, neurogenesis, and network connectivity highlight the dynamic feedback loop between cognitive processes and experience-dependent plasticity. There is a dynamic interplay between genetic predisposition and environmental and experiential factors. Learning as an isolated environmental factor shapes the brain. Individual learning trajectories emerge even when the "talent" is controlled for and are stable in response to different "teaching" interventions.

An experiment with our paradigm, in which the genetic background varies systematically (e.g., using a recombinant inbred panel of mice such as BXD, which we have used in the past (*28*), would be a major next step but would be so large, logistically complex, and expensive that it is now not conceivable and financeable. In theory, with such an approach, a genetics of the nonshared environment would be possible.

Variation in learning can also be observed under highly controlled conditions with traditional experimenter-guided behavioral tests. The International Brain Laboratory has published a across-lab comparison that revealed that there was initial variance in training, which diminished, when performance after training was compared. This was taken as argument that standardization is possible to improve lab-to-lab comparisons (*29*). The apparent subsequent reduction in variability, however, presumably reflected a ceiling effect, when the mice reach a criterion in the standardized test. This is fundamentally different from our case of self-paced learning in a series of tasks over weeks, in which—as we here show—task performance remains dependent on extrinsic cues and the reduction in variability is reversed, when the task changes again.

In our experiment, substantial individual differences emerged in the course of development, although genetic variance was minimized and the environment was kept uniform. We show that these long-term individual differences in the brain and behavior originated from individual differences in learning experiences. Our results indicate that equal opportunities and equal genes do not guarantee equal biographies. The consequences of this discovery for education and lifelong learning in humans are highly suggestive.

MATERIALS AND METHODS

Animal husbandry

All animal husbandry and experiments were conducted in accordance with the applicable European and national regulations (Tierschutzgesetz) and were approved by the local authority (Landesdirektion Sachsen; file number TVV8/2019). Female C57BL/6JRj mice at 5 weeks of age were purchased from Janvier Labs. At the animal facility of the German Center for Neurodegenerative Diseases (DZNE) Dresden, the mice were initially housed in standard cages in groups of four for 2 weeks for acclimatization. During the second week, half of the animals were randomly assigned to the IC group, and a glass-coated microtransponder (DataMars) was injected subcutaneously into the neck area. The other half were randomly allocated to four standard (STD) cages. All mice were kept on a 12-hour light/12-hour dark cycle and received water and food ad libitum. Cages were cleaned weekly. Four weeks before the end of the IC period, all mice were injected with the thymidine analog 5-chlorodeoxyuridine (CldU; dissolved in 0.9% sodium chloride) three times at 9-hour time intervals.

IntelliCage

The IC (TSE Systems, Bad Homburg, Germany), a computer-based, fully automated home cage system, was used for longitudinal monitoring of exploratory, learning, and social behavior of mice. The apparatus houses up to 16 mice and is equipped with four operant conditioning corners (hereafter "corners"), each of which contains two bottles of sweetened water as a reward, two nosepoke holes, and doors that allow or deny access to the reward. The software that controls the IC device enables the users to design specific learning protocols where access to reward is based on a predefined combination of factors, including visits to specific corners, nosepoke patterns, and animal identity. The time and duration of each behavioral event (corner visit, nosepoke, and lick), mouse ID, and corner ID were automatically recorded via RFID antennas, nosepoke sensors, and lickometers on the computer connected to the IC. Two paper houses and red plastic compartments were placed in the center of the IC. A water bottle was placed in the top grid of the cage next to the food so that the mice had ad libitum access to unsweetened water.

The following protocols were applied by appropriately designed modules in the IC apparatus:

1) Free adaptation: All doors were open, and the mice had free access to sweetened water in all corners of the IC.

2) Nosepoke adaptation: To access the reward, mice had to perform a nosepoke, which opened the respective door for 5 s. The mice had to leave the corner before they could reactivate the sensor to get to the reward again.

3) Drinking time adaptation: Access to the reward was restricted to a time window of 4.5 hours during the dark phase, from 10:30 p.m. to 3:00 a.m.

4) PL3CC: Access to the reward was restricted to only three corners upon performing a nosepoke.

5) PL1CC: Access to the reward was restricted to only one corner upon performing a nosepoke. The formerly incorrect corner became the only correct corner.

6) Patrolling with nosepoke: The position of the rewarded or correct corner shifted in either a clockwise or anticlockwise manner.

7) Reverse patrolling with nosepoke: The direction in which the correct corner rotated was reversed.

8) Serial reversal learning task: Initially, two diagonally opposite corners served as the rewarded corners, between which the mice had to shuttle to access the reward. The assignment of diagonally opposite correct and incorrect corners was reversed every 4 days.

9) Free days: On free days, no specific task took place, allowing the mice to rest without any learning protocols.

Large-scale CMOS-based biosensor and recording acquisition setup

To record pharmacologically induced and electrical stimulation-evoked responses, HD CMOS-based MEA chips were incorporated into an acquisition system (3Brain, AG, Switzerland). These HD CMOS chips comprise 4096 recording electrodes with a 42-μm

pitch size, forming an active sensing area of ~7 mm^2, which is sufficient for recording the entire hippocampal-cortical (HC) area. The on-chip amplification circuit is capable of band-pass filtering in the range of 0.1 to 5 kHz, achieved by a global gain of 60 dB to record both slow and fast oscillations. The aforementioned acquisition system was supplemented with a zero-drift triple-axis micromanipulator system (Sensapex, Finland) and a bipolar, platinum/iridium blunt microtip electrode (World Precision Instruments, Germany GmbH) for external on-chip electrical stimulation. To maintain slice health and minimize experimental variation, a heat-stabilized perfusion system (ALA Scientific Instruments, USA) delivered the appropriate oxygenated recording perfusate to the brain-chip interface at a flow rate of 4.5 ml/min and was kept temperature controlled at 37°C throughout the experiment.

Acute brain slice preparation and recovery

Following behavioral testing, mice from three groups ($n = 2$ each)—top and bottom behavioral performers from IC housing and controls from STD housing—were chosen for large-scale CMOS-based biosensor recordings. Mice were anesthetized with isoflurane before decapitation, and horizontal, 300-μm-thick brain slices were prepared using a Leica Vibratome VT1200S (Leica Microsystems, Germany) according to previous studies (*20*, *30*, *31*). Briefly, the brain was extracted from the skull and immediately immersed in a chilled sucrose solution. The brain was then positioned in a custom-made agarose-based container and affixed to the cutting plate. Horizontal brain slices were sectioned at 0° to 2°C and continuously perfused with a high-sucrose artificial cerebro-spinal fluid perfusate solution saturated with 95% O_2 and 5% CO_2. This high-sucrose perfusate contained in 250 mM sucrose, 10 mM glucose, 1.25 mM NaH_2PO_4, 24 mM $NaHCO_3$, 2.5 mM KCl, 0.5 mM ascorbic acid, 4 mM $MgCl_2$, 1.2 mM $MgSO_4$, and 0.5 mM $CaCl_2$ (pH = 7.30 to 7.40; 350 to 360 mOsm/liter).

Electrical stimulation-evoked response recordings

HC slices were incubated at 32°C for 45 min, followed by a recovery at room temperature for 1 hour in an aCSF recording perfusate solution saturated with 95% O_2 and 5% CO_2. The aCSF perfusate contained in 127 mM NaCl, 3.5 mM KCl, 1.25 mM NaH_2PO_4, 26 mM $NaHCO_3$, 10 mM glucose, 1 mM $MgSO_4$, and 2.5 mM $CaCl_2$ (pH = 7.25 to 7.35; 305 to 315 mOsm/liter). Slices were then moved and coupled onto the HD CMOS chips using a custom platinum anchor placed on top of the tissue. To determine external electrode placement for electrical stimulation, an optical imaging stereomicroscope (Leica Microsystems, Germany) was connected to the CMOS-based biosensor to capture HC brain slice structures. The electrode was placed in the stratum radiatum of the CA1 to activate the SC pathway and elicit fEPSPs (*30*). To confirm electrode placement in this pathway, a monophasic, 60-μA pulse with a pulse half-width of 140 μs was applied, and the responses were recorded. To determine the intensity of evoked responses, a tuning curve was established using a 10-μA stepwise stimulation application from 20 to 130 μA applied at 30-s intervals. These evoked synaptic responses were integrated into offline analysis with the microscope images described previously to obtain the spatial arrangement of tissue relative to the recording during offline analysis. To characterize specific synaptic function, active electrodes were grouped offline based on statistically determined bioelectrical signal differences using EVOS software (3Brain AG, Switzerland). Specifically, fEPSP signals obtained from the stratum radiatum and stratum pyramidale were analyzed.

Pharmacologically induced response recordings

HC slices were incubated at 32°C for 45 min, followed by a recovery at room temperature for 1 hour in an aCSF recording perfusate solution saturated with 95% O_2 and 5% CO_2. This aCSF perfusate contained in 127 mM NaCl, 2.5 mM KCl, 1.25 mM NaH_2PO_4, 24 mM $NaHCO_3$, 25 mM glucose, 1.25 mM $MgSO_4$, and 2 mM $CaCl_2$ (pH = 7.25 to 7.35; 315 to 325 mOsm/liter). Slices were then moved and coupled onto the HD CMOS chips using a custom platinum anchor placed on top of the tissue. Ten minutes of spontaneous and 5 min of pharmacologically induced extracellular recordings were collected at a 14 kHz per electrode sampling frequency. Pharmacologically induced circuit activation recordings were acquired through the application of 100 μM 4-aminopyridine. A stereomicroscope captured brain slice structures through optical imaging, which were used to obtain the spatial arrangement of tissue relative to extracellular recordings during offline analysis.

Tissue preparation and immunohistochemistry

Mice were deeply anesthetized with a mixture of ketamine (100 mg/kg) and xylazine (10 mg/kg) and then transcardially perfused with 0.9% saline and 4% paraformaldehyde (PFA) in phosphate buffer (pH 7.4). Brains were removed from the skull, left in 4% PFA overnight at 4°C, and transferred to 30% sucrose for at least 2 days. Forty-micrometer coronal sections were obtained using a sliding microtome with a dry ice–cooled copper block (Leica, SM2000R). Brain sections were stored at 4°C in cryoprotectant solution (25% ethylene glycol and 25% glycerol in 0.1 M phosphate buffer; pH 7.4). For the detection of CldU-positive cells, the peroxidase method was applied. Free-floating sections were first incubated in 0.6% hydrogen peroxide for 30 min to inhibit endogenous peroxidase activity. For antigen retrieval, the sections were then incubated in preheated 2.5 M hydrochloric acid for 30 min at 37°C, followed by thorough washing steps. To block unspecific binding sites, the sections were treated with tris-buffered saline (TBS) supplemented with 10% donkey serum and 0.2% Triton X-100 (Carl Roth) for 1 hour at room temperature. Next, the sections were incubated with primary monoclonal rat anti-CldU antibody (1:500) overnight at 4°C followed by biotinylated secondary antibodies for 2 hours at room temperature. Antibodies were diluted in TBS supplemented with 3% donkey serum and 0.2% Triton X-100. For the detection of CldU-positive cells, the VECTASTAIN Elite ABC Reagent with diaminobenzidine (0.075 mg/ml; Sigma-Aldrich) and 0.04% nickel chloride as a chromogen were used. All washing steps were performed using TBS. The stained sections were mounted onto glass slides, cleared with Neo-Clear (Millipore), and lastly cover-slipped using Neo-Mount (Millipore). CldU-positive cells were counted on every sixth section along the entire rostro-caudal axis of the DG using a bright-field microscope.

Electrophysiology data analysis

All further analyses used in this study were developed and implemented with custom-written Python scripts. Package add-ons are cited accordingly. All statistical analyses were performed with OriginLab 2022.

HC structural clusters

To characterize hippocampal network behavior locally and globally, functional firing electrodes were overlaid on the corresponding brain slice images to obtain structure-function information. Electrodes were then grouped on the basis of annotated structural markers on the HC slice. These structures included seven regions of the

HC circuit: DG infrapyramidal blade, DG suprapyramidal blade, hilus, CA1, CA3, entorhinal cortex, and perirhinal cortex.

Mean activity basic analysis

To examine specific LFP waveform patterns, LFP event detection was performed using a hard threshold algorithm. Events were denoised and filtered using a low-pass fourth order Butterworth filter (1 to 100 Hz) processed by a custom-written Python script. The signal amplitude analysis was obtained through full-wave rectification and low-pass filtering with a cutoff frequency of 100 Hz.

Functional connectivity and causality

Cross-covariance was calculated between pairs of electrodes in the 64 by 64 array using Pearson's correlation coefficient to infer large-scale statistically dependent connectivity on a multilayered hippocampal network. Multivariate Granger causality was performed to quantify the influence of one time series on another followed by directed transfer function to measure directional information flow (*20*, *30*–*32*). Electrodes were sorted by HC regions, and the statistical calculations for the count of interconnection links were based on paired layers.

Network connectivity metrics

To describe the overall network topology and interconnectedness from LFP events, graph theoretic analyses were applied. Graph metrics were computed in custom-written Python code with adapted functions from NetworkX Python package (*32*, *33*), available on GitHub (https://github.com/networkx). Briefly, functional network connectivity metrics are described by considering node n as the central potentially connected component of the graph, which in our case corresponds to a specific electrode in the sensing array. The edges e are the functional links or connections between each node n. Other metrics, such as degree, degree centrality, clustering coefficient, average shortest path length, and transitivity, are described (*20*).

Graph map visualization

To visualize the large-scale network, connectivity maps were constructed with the data architecture containing nodes and edges using the Gephi program 9.2 version (https://gephi.org). To illustrate exemplary functional connectivity from the dynamic detected LFP events in each condition, similar dynamic timeline (100 s) and degree range (>10 functional links per node) parameter constraints were placed on the functional links for plotting each condition. Nodes are scaled according to degree strength and sorted on the basis of each structural layer.

Behavioral analysis

The IC software outputs a raw data file with descriptive information about each animal's visit to the corners, which allows the computation of the variables per day listed below. In the adaptation phase, exploratory activity was examined by calculating RE. Corner visit durations were converted to probabilities $p_{i,j,t}$ of a mouse i being found at a corner j on a day t. Shannon entropy of the roaming distribution was calculated as $RE_{i,t} = -\sum_{j=0}^{4} p_{i,j,t}\log\left(p_{i,j,t}\right)/\log(4)$. Dividing the entropy by log(4) which is the number of corners in the IC scales the RE to the range between zero and one. Cumulative RE was calculated by the cumulative addition of mean RE from the previous days. In the learning phase, the percentage of correct visits (correct visits/total visits × 100) was used as a metric to analyze learning behavior of individual mice during all tasks. A correct visit is defined as a visit to a correct corner followed by more than one nosepoke which indicates a reward-seeking behavior as opposed to just exploratory behavior. To assess the flexibility of individual mice in forgetting the previous learning rule when a new task starts, we calculated the percentage of times mice visited the previously assigned correct corner (visits to correct corners of previous task/total visits × 100).

Simulation and comparison of reinforcement and null models

To test whether the emergence of variance in our data is due to learning reinforcement and not to the amplification of stochastic initial differences through developmental noise, we simulated a reinforcement model and compared it to null models using bootstrap analysis.

Two null models were used. In the random walk model, the success in the trials is obtained from a random distribution around the initial differences. In the additive noise model, the success in the current trial is the sum of success in the previous trial plus noise. This model simulates the hypothesis that interindividual differences emerge as a result of stochasticity or noise during development which is then canalized as a result of the developmental process.

For the simulations, 16 mice underwent a series of trials—50 trials for the learning phase and 10 for exploration. Each mouse was assigned a different baseline or intercept, randomly selected from ranges based on our experimental data: between −0.27 and 0.43 for learning and between 0.09 and 0.16 for exploration. In the reinforcement model, each mouse also received a unique reinforcement factor, randomly chosen from ranges of [−0.011, 0.045] for learning and [−0.0063, 0.00024] for exploration, again derived from our experimental observations. The stochastic noise was set equal to the maximum value of the reinforcement factor, which was 0.045 for learning and 0.00024 for exploration.

The behavioral response in the different models was calculated as

Random walk model

$$\%\text{CorrectVisits}_{(t+1)} = \text{NormalDistribution}\left(\mu = \text{Baseline}, \sigma^2 = \text{Noise}\right) \quad (1)$$

$$\text{RE}_{(t+1)} = \text{NormalDistribution}\left(\mu = \text{Baseline}, \sigma^2 = \text{Noise}\right) \quad (2)$$

Additive noise model

$$\%\text{CorrectVisits}_{(t+1)} = \%\text{CorrectVisits}_{(t)} + \text{Noise} \quad (3)$$

$$\text{RE}_{(t+1)} = \text{RE}_{(t)} + \text{Noise} \quad (4)$$

Reinforcement model

$$\%\text{CorrectVisits}_{(t+1)} = \%\text{CorrectVisits}_{(t)} + \text{ReinforcementFactor} + \text{Noise} \quad (5)$$

$$\text{RE}_{(t+1)} = \text{RE}_{(t)} + \text{ReinforcementFactor} + \text{Noise} \quad (6)$$

We performed a bootstrap analysis with 1000 simulations to compare the slopes of change in mean and variance between the three models. For each bootstrap iteration, we fit regression models to the mean and variance changes over time. We then calculated the pairwise differences in slopes between the three models for each simulation, yielding a bootstrap distribution that reflects the variability in slope differences due to baseline variability and noise.

To assess the significance of the differences, we calculated the 95% CIs for the slope differences by identifying the 2.5th and 97.5th percentiles of the bootstrap distribution. In addition, *P* values were computed by determining the proportion of bootstrap iterations where the slope difference was equal to or less than zero.

Statistical analysis

Statistical analyses were conducted using the R software (R Core Team, 2014). To compare longitudinal data means, we used a rank-based nonparametric test, using the "nparLD" function from the nparLD package (*34*). This test provides analysis of variance (ANOVA)–type statistics for time, group, and their interaction. Post hoc pairwise comparisons were executed using the Wilcoxon's test. Variances between groups were compared using the Brown-Forsythe test, conducted with the "leveneTest" function from the "car" package. All statistical tests were two-tailed, and significance was considered at $P < 0.05$. To correct for multiple comparisons, the Holm-Bonferroni method was used.

The data visualizations were generated using the "ggplot2" package (*35*). In the box-whisker plots, the centerline represents the median. The upper and lower hinges indicate the first and third quartiles, respectively. The upper whisker extends from the hinge to the largest value within 1.5 times the interquartile range (IQR), while the lower whisker extends from the hinge to the smallest value within 1.5 times the IQR.

For longitudinal analysis of RE, learning and flexibility for individual mice, linear mixed-effect models were used from the "lme4" package (*36*). Mouse identity was added as a random effect to the within-subject factor (i.e., repeated measure) and between-subject fixed effects. To estimate repeatability (R) which is the relative decomposition of variance into interindividual and intraindividual variance $[R = (\text{interindividual variance})/(\text{interindividual variance} + \text{intraindividual variance})]$, "rptR" package was used (*37*).

Supplementary Materials

This PDF file includes:

Figs. S1 to S6
Tables S1 to S7

REFERENCES AND NOTES

1. S. D. Gosling, From mice to men: What can we learn about personality from animal research? *Psychol. Bull.* **127**, 45–86 (2001).
2. A. Sih, A. M. Bell, J. C. Johnson, R. E. Ziemba, Behavioral syndromes: An integrative overview. *Q. Rev. Biol.* **79**, 241–277 (2004).
3. G. Kempermann, J. B. Lopes, S. Zocher, S. Schilling, F. Ehret, A. Garthe, A. Karasinsky, A. M. Brandmaier, U. Lindenberger, Y. Winter, R. W. Overall, The individuality paradigm: Automated longitudinal activity tracking of large cohorts of genetically identical mice in an enriched environment. *Neurobiol. Dis.* **175**, 105916 (2022).
4. K. Honegger, B. de Bivort, Stochasticity, individuality and behavior. *Curr. Biol.* **28**, R8–R12 (2018).
5. D. Bierbach, K. L. Laskowski, M. Wolf, Behavioural individuality in clonal fish arises despite near-identical rearing conditions. *Nat. Commun.* **8**, 15361 (2017).
6. D. N. Fisher, M. Brachmann, J. B. Burant, Complex dynamics and the development of behavioural individuality. *Anim. Behav.* **138**, e1–e6 (2018).
7. A. Kiryk, A. Janusz, B. Zglinicki, E. Turkes, E. Knapska, W. Konopka, H.-P. Lipp, L. Kaczmarek, IntelliCage as a tool for measuring mouse behavior – 20 years perspective. *Behav. Brain Res.* **388**, 112620 (2020).
8. J. C. Körholz, S. Zocher, A. N. Grzyb, B. Morisse, A. Poetzsch, F. Ehret, C. Schmied, G. Kempermann, Selective increases in inter-individual variability in response to environmental enrichment in female mice. *eLife* **7**, e35690 (2018).
9. G. Kempermann, H. G. Kuhn, F. H. Gage, More hippocampal neurons in adult mice living in an enriched environment. *Nature* **386**, 493–495 (1997).
10. J. Freund, A. M. Brandmaier, L. Lewejohann, I. Kirste, M. Kritzler, A. Krüger, N. Sachser, U. Lindenberger, G. Kempermann, Emergence of individuality in genetically identical mice. *Science* **340**, 756–759 (2013).
11. S. Zocher, S. Schilling, A. N. Grzyb, V. S. Adusumilli, J. Bogado Lopes, S. Günther, R. W. Overall, Y. Winter, G. Kempermann, Early-life environmental enrichment generates persistent individualized behavior in mice. *Sci. Adv.* **6**, eabb1478 (2020).
12. A. S. Heller, T. C. Shi, C. E. C. Ezie, T. R. Reneau, L. M. Baez, C. J. Gibbons, C. A. Hartley, Association between real-world experiential diversity and positive affect relates to hippocampal–striatal functional connectivity. *Nat. Neurosci.* **23**, 800–804 (2020).
13. J. Bogado Lopes, A. N. Senko, K. Bahnsen, D. Geisler, E. Kim, M. Bernanos, D. Cash, S. Ehrlich, A. C. Vernon, G. Kempermann, Individual behavioral trajectories shape whole-brain connectivity in mice. *eLife* **12**, e80379 (2023).
14. J. B. Lopes, M. Małz, A. N. Senko, S. Zocher, G. Kempermann, Loss of individualized behavioral trajectories in adult neurogenesis-deficient cyclin D2 knockout mice. *Hippocampus* **33**, 360–372 (2023).
15. G. Berdugo-Vega, C.-C. Lee, A. Garthe, G. Kempermann, F. Calegari, Adult-born neurons promote cognitive flexibility by improving memory precision and indexing. *Hippocampus* **31**, 1068–1079 (2021).
16. A. Garthe, J. Behr, G. Kempermann, Adult-generated hippocampal neurons allow the flexible use of spatially precise learning strategies. *PLOS ONE* **4**, e5464 (2009).
17. A. Garthe, I. Roeder, G. Kempermann, Mice in an enriched environment learn more flexibly because of adult hippocampal neurogenesis. *Hippocampus* **26**, 261–271 (2016).
18. R. H. Thaler, C. R. Sunstein, *Nudge: Improving Decisions About Health, Wealth, and Happiness* (Penguin, 2009).
19. N. J. Dingemanse, N. A. Dochtermann, Quantifying individual variation in behaviour: Mixed-effect modelling approaches. *J. Anim. Ecol.* **82**, 39–54 (2013).
20. B. A. Emery, X. Hu, S. Khanzada, G. Kempermann, H. Amin, High-resolution CMOS-based biosensor for assessing hippocampal circuit dynamics in experience-dependent plasticity. *Biosens. Bioelectron.* **237**, 115471 (2023).
21. W. C. Abraham, O. D. Jones, D. L. Glanzman, Is plasticity of synapses the mechanism of long-term memory storage? *NPJ Sci. Learn.* **4**, 9 (2019).
22. K. Cassady, H. Gagnon, P. Lalwani, M. Simmonite, B. Foerster, D. Park, S. J. Peltier, M. Petrou, S. F. Taylor, D. H. Weissman, R. D. Seidler, T. A. Polk, Sensorimotor network segregation declines with age and is linked to GABA and to sensorimotor performance. *Neuroimage* **186**, 234–244 (2019).
23. R. Pedersen, L. Geerligs, M. Andersson, T. Gorbach, B. Avelar-Pereira, A. Wåhlin, A. Rieckmann, L. Nyberg, A. Salami, When functional blurring becomes deleterious: Reduced system segregation is associated with less white matter integrity and cognitive decline in aging. *Neuroimage* **242**, 118449 (2021).
24. M. Rubinov, O. Sporns, Complex network measures of brain connectivity: Uses and interpretations. *Neuroimage* **52**, 1059–1069 (2010).
25. A. Sih, K. J. Mathot, M. Moirón, P.-O. Montiglio, M. Wolf, N. J. Dingemanse, Animal personality and state–behaviour feedbacks: A review and guide for empiricists. *Trends Ecol. Evol.* **30**, 50–60 (2015).
26. G. Kempermann, Environmental enrichment, new neurons and the neurobiology of individuality. *Nat. Rev. Neurosci.* **20**, 235–245 (2019).
27. P. C. M. Molenaar, D. I. Boomsma, C. V. Dolan, A third source of developmental differences. *Behav. Genet.* **23**, 519–524 (1993).
28. G. Kempermann, E. J. Chesler, L. Lu, R. W. Williams, F. H. Gage, Natural variation and genetic covariance in adult hippocampal neurogenesis. *Proc. Natl. Acad. Sci. U.S.A.* **103**, 780–785 (2006).
29. International Brain Laboratory, V. Aguillon-Rodriguez, D. Angelaki, H. Bayer, N. Bonacchi, M. Carandini, F. Cazettes, G. Chapuis, A. K. Churchland, Y. Dan, E. Dewitt, M. Faulkner, H. Forrest, L. Haetzel, M. Häusser, S. B. Hofer, F. Hu, A. Khanal, C. Krasniak, I. Laranjeira, Z. F. Mainen, G. Meijer, N. J. Miska, T. D. Mrsic-Flogel, M. Murakami, J.-P. Noel, A. Pan-Vazquez, C. Rossant, J. Sanders, K. Socha, R. Terry, A. E. Urai, H. Vergara, M. Wells, C. J. Wilson, I. B. Witten, L. E. Wool, A. M. Zador, Standardized and reproducible measurement of decision-making in mice. *eLife.* **10**, e63711 (2021).
30. B. A. Emery, S. Khanzada, X. Hu, L. Rossi, D. Klütsch, E. Altuntac, H. Amin, Recording Network-based Synaptic Transmission and LTP in the Hippocampal Network on a Large-scale Biosensor, in *2023 IEEE BioSensors Conference (BioSensors)* (IEEE, 2023; https://ieeexplore.ieee.org/document/10280958/), pp. 1–4.
31. X. Hu, S. Khanzada, D. Klütsch, F. Calegari, H. Amin, Implementation of biohybrid olfactory bulb on a high-density CMOS-chip to reveal large-scale spatiotemporal circuit information. *Biosens. Bioelectron.* **198**, 113834 (2022).
32. B. A. Emery, X. Hu, L. Maugeri, S. Khanzada, D. Klütsch, E. Altuntac, H. Amin, Large-scale Multimodal Recordings on a High-density Neurochip: Olfactory Bulb and Hippocampal Networks, in *2022 44th Annual International Conference of the IEEE Engineering in Medicine*

& Biology Society (EMBC) (IEEE, 2022), pp. 3111–3114; https://ieeexplore.ieee.org/abstract/document/9871961.
33. A. Hagberg, P. J. Swart, D. A. Schult, Exploring network structure, dynamics, and function using NetworkX, (LA-UR-08-05495; LA-UR-08-5495, Los Alamos National Laboratory (LANL), Los Alamos, NM (United States), 2008); https://osti.gov/biblio/960616.
34. K. Noguchi, Y. R. Gel, E. Brunner, F. Konietschke, nparLD: An R software package for the nonparametric analysis of longitudinal data in factorial experiments. *J. Stat. Softw.* **50**, 1–23 (2012).
35. H. Wickham, "Data analysis" in *Ggplot2: Elegant Graphics for Data Analysis*, H. Wickham, Ed. (Springer International Publishing, 2016; https://doi.org/10.1007/978-3-319-24277-4_9, pp. 189–201.
36. D. Bates, M. Mächler, B. Bolker, S. Walker, Fitting linear mixed-effects models using lme4. *J. Stat. Softw.* **67**, 1–48 (2015).
37. M. A. Stoffel, S. Nakagawa, H. Schielzeth, rptR: Repeatability estimation and variance decomposition by generalized linear mixed-effects models. *Methods Ecol. Evol.* **8**, 1639–1644 (2017).

Acknowledgments: We thank all members of the Kempermann lab for assistance with the experiments; S. Guenther and J. Bergmann for animal care; A. Karasinsky, D. Lasse, and C. Steinhauer for help with CldU immunohistochemistry. We thank S. Barde for drawing the IC in Fig. 1A and U. Lindenberger and F. H. Gage for valuable discussion of the findings. **Funding:** This project was in part supported by the grant "The mouse in the supermarket" from Volkswagen Foundation. Otherwise, the project was financed with basic institutional funds. W.B. was supported by the International Max Planck Research School on the Life Course (LIFE, https://imprs-life.mpg.de/; participating institutions: Max Planck Institute for Human Development, Freie Universität Berlin, Humboldt-Universität zu Berlin, University of Michigan, University of Virginia, and University of Zurich) **Author contributions:** Conceptualization: W.B., J.R., A.G., A.E.R., and G.K. Methodology: W.B., J.R., X.H., A.G., H.A., and G.K. Investigation: W.B., J.R., B.E., S.K., X.H., and A.H. Visualization: W.B., H.A., A.E.R., and G.K. Funding acquisition: H.A. and G.K. Project administration: A.E.R. and G.K. Supervision: A.E.R., H.A., and G.K. Writing—original draft: W.B. and G.K. Writing—review and editing: W.B., A.E.R., H.A., and G.K. **Competing interests:** The authors declare that they have no competing interests. **Data and materials availability:** The behavioral data underlying this study are available on Dryad under the following link: https://doi.org/10.5061/dryad.xgxd254rb. All data needed to evaluate the conclusions in the paper are present in the paper and/or the Supplementary Materials.

Submitted 26 August 2024
Accepted 6 December 2024
Published 10 January 2025
10.1126/sciadv.ads7297